


Article

Comparison of Flood Frequency at Different Climatic Scenarios in Forested Coastal Watersheds

Shreeya Bhattarai, Prem B. Parajuli *  and Filip To

Department of Agricultural and Biological Engineering, Mississippi State University, Mississippi State, Starkville, MS 36762, USA

* Correspondence: pparajuli@abe.msstate.edu

Abstract: Climate change-induced extreme precipitation causes coastal flooding. A streamflow simulation in coastal watersheds, Wolf River Watershed (WRW) and Jourdan River Watershed (JRW), was conducted using the Soil and Water Assessment Tool (SWAT) to compare variation in flow at different climates and to analyze the flood frequency. Baseline models were auto-calibrated with SWAT calibration and uncertainty programs (SWAT-CUP). Kling–Gupta efficiency (KGE), defined as the objective function in SWAT-CUP, ranged from 0.8 to 0.7 in WRW and from 0.55 to 0.68 in JRW during the calibration–validation process. Results indicated reliability of the model performances. Monthly averaged baseline flow was 1% greater than historical and 8.9% lower than future climate in WRW. In JRW, monthly averaged baseline flow was 11% greater than historical and 5.7% lower than future climate. Flood frequency analysis showed the highest 1% exceedance probability in annual maximum series (AMS) of baseline model in WRW, whereas AMS of projected model was estimated the highest in JRW. This study aids in preparing for future flood management.

Keywords: streamflow; SWAT; climate change; CMIP5; CMHyd; peak flow; annual maximum series; partial duration series; flood frequency analysis; Log Pearson type III



Citation: Bhattarai, S.; Parajuli, P.B.; To, F. Comparison of Flood Frequency at Different Climatic Scenarios in Forested Coastal Watersheds. *Climate* **2023**, *11*, 41. <https://doi.org/10.3390/cli11020041>

Academic Editor: Nir Y. Krakauer

Received: 16 December 2022

Revised: 6 February 2023

Accepted: 6 February 2023

Published: 9 February 2023



Copyright: © 2023 by the authors. Licensee MDPI, Basel, Switzerland. This article is an open access article distributed under the terms and conditions of the Creative Commons Attribution (CC BY) license (<https://creativecommons.org/licenses/by/4.0/>).

1. Introduction

The frequency and severity of weather extremes are rising due to climate change [1]. Climate change causes variations in streamflow [2], triggering more frequent flooding events [3]. In the 21st century, extreme precipitation events are predicted to become more frequent, surpassing the present magnitude [4]. According to the Fifth Assessment Report of the Intergovernmental Panel on Climate Change (IPCC), climate change is projected to increase the risk of storms, extreme precipitation, flooding, and storm surges in coastal regions [5]. Moreover, there is an increasing trend in the population in coastal areas and the global population is projected to be more than 1 billion by the mid-21st century in the low-elevated coastal zone [6]. This poses a high risk of extreme events to the public and property on the coast [7]. Risk assessment of flood-prone areas can be carried out using a hydrological modelling approach [8–12]. Hydrological assessment of coastal plains is essential to study the quantity of streamflow, predict the occurrence of extreme events, analyze its trend in different climatic conditions, and understand the impact of climate change on the discharge of coastal rivers.

Extensive research has been conducted in flood risk assessment, which led to the development of numerous mathematical modelling tools over time [13], for instance, the Soil and Water Assessment Tool (SWAT) [8,11,14], Modélisation de l'Anticipation du Ruissellement et des Inondations pour des événements Extrêmes (MARINE) model [8,15], Hydrologic Engineering Center-River Analysis System (HEC-RAS) [9,16,17], Hydrologic Engineering Center-Hydrologic Modeling System (HEC-HMS) [9,18], a two-dimensional watershed rainfall-runoff CASC2D model [10,19], TOPography-based hydrological MODEL (TOPMODEL) [12,20], MIKE FLOOD [12,21], among others. The flood risk analysis by

Ajmal et al. [22] compared the hydrological, hydro-dynamical, and hybrid tools, and concluded that all models can be used in different scenarios depending on the water level area. Hydrologic models are effective tools for watershed management planning and climate change analysis [22].

SWAT is a semi-distributed hydrologic model [14] capable of modelling future floods [23] on a watershed scale. It can also be used with space-based flood detection components for flood risk analysis in ungagged watersheds [24]. As of December 2022, over 5500 publications were recorded in the SWAT database (https://www.card.iastate.edu/swat_articles/, accessed on 1 December 2022) [25] regarding its development and application. SWAT has been used in numerous global studies at different time steps to investigate the climate change impact on hydrological processes [26–30]. In previous studies, the SWAT model has been applied for hydro-climatological research [31,32] and successfully conducted flood frequency analysis [33,34]. The hydrological modelling tools can account for the complex system of hydrology, quantify the variation in streamflow and predict the flood-causing potential peak flow events. In this study, the SWAT model was applied to coastal watersheds where flood frequency analysis is crucial to assess the risk of weather extreme events in the coastal settlement. Although SWAT is limited to simulating the tidal influence into the coastal watershed [35], watershed delineated further upstream tends to have no influence of the tides; therefore, it is not considered in the context of this study.

The hydrological cycle is affected by climate change [36]. Since the earth's temperature drives evaporation, condensation, and precipitation, climate change is likely to disrupt the hydrological balance. Evidence of a rise in average temperature in recent decades [37] directly relates to an increase in water vapor content in the atmosphere, leading to intense rainfall in the coastal area. The coastal watersheds of Mississippi are vulnerable to extreme weather events. Severe storms, tornadoes, flood incidents, and hurricanes were declared among the 29 major disasters by the Federal Emergency Management Agency between 2005–2020 in the state of Mississippi [38]. High precipitation is recorded over the years in the Mississippi coastal watersheds [39,40] that drain into the Mississippi Sound and eventually onto the Gulf of Mexico. Therefore, the objectives of this study were to: (i) set up baseline SWAT models for two forested coastal watersheds; (ii) set up a SWAT model for historical and projected climate conditions; (iii) compare the variation in streamflow during different climatic conditions with respect to the baseline model; and (iv) analyze the flood frequency of the stream at different climatic extremities.

2. Materials and Methods

2.1. Study Area

This study was conducted in two forested watersheds: Wolf River Watershed (WRW) and Jourdan River Watershed (JRW) of Mississippi, United States of America. The Wolf River and the Jourdan River run through the coastal plain; thus, these are categorized as coastal streams which fetch fresh water to Saint Louis Bay (SLB). WRW lies between the latitude of 31°5' N and 30°27' N and longitude of 89°35' W and 89°15' W. JRW lies between the latitude of 30°44' N and 30°22' N and longitude of 89°38' W and 89°22' W. Both watersheds are close to the Gulf of Mexico and are frequently impacted by extreme weather events. WRW covers an area of 801 km² and the land use is dominated by forest. The land use of WRW consists of 46.6% forest–evergreen, 24.9% range–brush, 20.8% wetlands–forested, and 7.7% pasture. Similarly, the land use of JRW is also dominated by forest. The total area of JRW is 538 km² and it consists of 37.9% forest–evergreen, 26.6% range–brush, 18.26% pasture, and 17.3% wetlands–forested. Figure 1 shows the location map of WRW and JRW in the state of Mississippi. Mississippi has a humid subtropical climate. The annual average temperature at SLB is 19.9 °C, with an average precipitation of 1534.2 mm annually occurring on an average of 98 rainy days throughout the year.

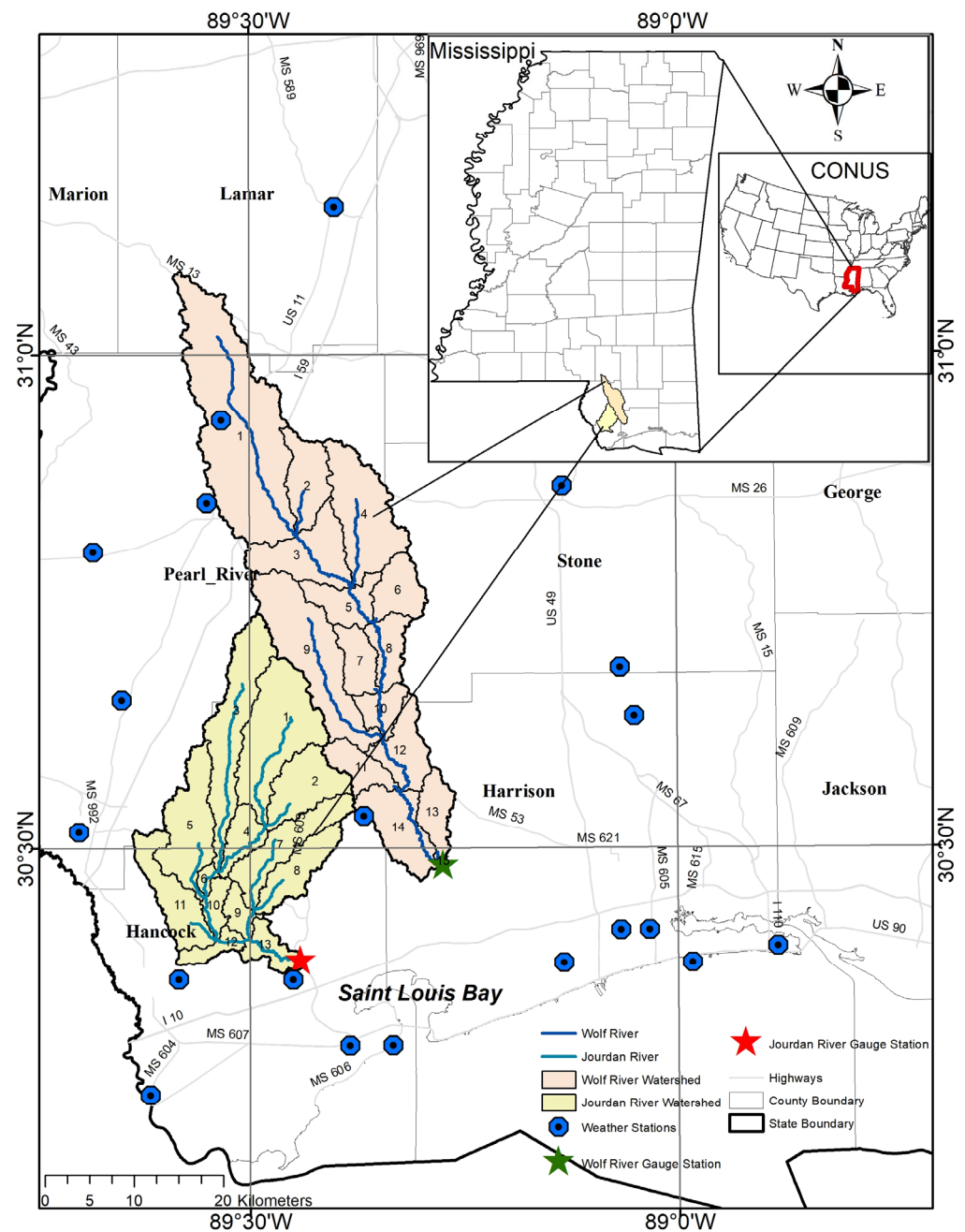


Figure 1. Study area map of the Wolf River Watershed and Jourdan River Watershed in Mississippi. (CONUS: continental United States).

2.2. Model Setup

Soil and Water Assessment Tool (SWAT) [14], a watershed-scale conceptual process-based model, was applied to the two adjacent watersheds for evaluating the streamflow from the coastal plain. GIS-coupled public domain software ArcSWAT is popular worldwide for hydrological modelling [41]. In the SWAT model, the hydrological analysis is carried out by dividing a watershed into smaller sub-watersheds and further into discrete hydrological response units (HRUs) on the basis of the unique combination of its land use, soil, and slope type [42]. For both watersheds, a baseline model was developed from 1995 to 2010. Additionally, a historical model from 1950 to 1994 and a projected model from 2011 to 2055 were developed to create different climatic conditions for each watershed. Thus, six different SWAT models were developed to study the hydrologic response of past and

future climatic conditions ranging 45 years into the past and 45 years into the future from the baseline model. The basic data used to develop the baseline models are listed in Table 1.

Table 1. Data for the development of baseline SWAT model.

S. No.	Data	Source
1	Elevation Data: Digital Elevation Model (DEM) (30 m × 30 m) (2020)	United States Geological Survey (USGS) (http://viewer.nationalmap.gov/viewer/) (accessed on 4 October 2022)
2	Land-use and Land-cover Data: Cropland Data Layer (CDL) (2010)	United States Department of Agriculture-National Agricultural Statistics Service (USDA-NASS) (http://nassgeodata.gmu.edu/CropScape/) (accessed on 4 October 2022)
3	Soil Data: USSURGO (2020)	United States Soil Survey Geographic Database (US-SSURGO) SWAT-USSURGO (https://swat.tamu.edu/data/) (accessed on 4 October 2022)
4	Weather Data: NOAA (1995–2010) Precipitation, Maximum Temperature, Minimum Temperature Discharge Data:	National Oceanic and Atmospheric Administration (NOAA) SWAT—Climate Data (https://swat.tamu.edu/data/) (accessed on 4 October 2022)
5	-USGS 02481510 (1997–2010) (Wolf River Nr Landon) -USGS 02481660 (2002–2005) (Jourdan River Nr Bay St Louis)	United States Geological Survey (USGS) (https://waterdata.usgs.gov/ms/nwis/) (accessed on 5 October 2022)

The basic data used to develop the baseline models were the 2020 United States Geological Survey (USGS) Digital Elevation Model (DEM) data (30 m × 30 m resolution) (<http://viewer.nationalmap.gov/viewer/>, accessed on 4 October 2022) [43], the 2020 United States Soil Survey Geographic Database (US-SSURGO) (<https://swat.tamu.edu/data/>, accessed on 4 October 2022) [44], the 2010 Cropland Data Layer (CDL) United States Department of Agriculture-National Agricultural Statistics Service (USDA-NASS) (<http://nassgeodata.gmu.edu/CropScape/>, accessed on 4 October 2022) [45], and the 1995–2010 Weather Data-National Oceanic and Atmospheric Administration (NOAA) Climate Data (<https://swat.tamu.edu/data/>, accessed on 4 October 2022) [44]. Monthly discharge data were utilized, collected from USGS 02481510 Wolf River near Landon, MS (1997–2010), for WRW flow simulation, whereas daily discharge data were utilized from USGS 02481660 Jourdan River near Bay St Louis, MS (2002–2005), for JRW flow simulation due to the availability of limited data in this gauge station.

DEM, CDL, and USSURGO soil data were fed into the model and the slope classes were defined. A total of 801 km² WRW was divided into 15 subbasins and 489 HRUs, and 538 km² JRW was divided into 13 subbasins and 233 HRUs. The meteorological dataset from NOAA, retrieved from the SWAT website, was used as local weather data for precipitation and temperature data (at 21 stations for WRW spanning over five counties, and at 12 stations for JRW spanning over two counties). The baseline model for both WRW and JRW was then set up and run for 16 years (1995–2010) with a two-year warmup period each. The simulation was performed monthly for WRW and daily for JRW. SWAT calibration and uncertainty program (SWAT-CUP) Sufi-2 [46] was used for the uncertainty analysis of hydrological parameters and to calibrate–validate the baseline model of both watersheds. This widely used autocalibration tool was considered in this study because of its simpler calibration procedure, availability of essential hydrological parameters, uncertainty analysis, and sensitivity analysis features [46,47]. Kling–Gupta efficiency (KGE) [48] was used as the objective function in SWAT-CUP for more accurate model calibration. Monthly streamflow calibration was conducted from January 1997 to December 2003 and validation was carried out from January 2004 to December 2010 for WRW at USGS 02481510. Similarly, daily

streamflow calibration was conducted from 10 March 2002 to 31 December 2003 and validation was carried out from 1 January 2004 to 30 September 2004 with all the available data at the USGS 02481660 for JRW. The fitted parameters for the calibrating–validating baseline model of both watersheds are listed in Tables 2 and 3, respectively.

Table 2. Parameters used in streamflow calibration for Wolf River Watershed.

Parameters	Description	Fitted Value
CN2	Initial SCS runoff curve number for moisture condition II.	0.133
ALPHA_BF	Baseflow alpha factor (days).	0.316
ESCO	Soil evaporation compensation factor.	0.217
SOL_K	Saturated hydraulic conductivity.	−0.018
SOL_BD	Moist bulk density.	0.104
SOL_AWC	Available water capacity of the soil layer.	0.297

Table 3. Parameters used in streamflow calibration for Jourdan River Watershed.

Parameters	Description	Fitted Value
ALPHA_BF	Baseflow alpha factor (days).	0.917
ESCO	Soil evaporation compensation factor.	0.910
GW_DELAY	Groundwater delay (days).	1.126
GWQMN	Threshold depth of water in the shallow aquifer required for return flow to occur (mm).	874.982
EPCO	Plant uptake compensation factor.	0.698
CN2	Initial SCS runoff curve number for moisture condition II.	−0.194
RCHRG_DP	Deep aquifer percolation fraction.	0.391
REVAPMN	Threshold depth of water in the shallow aquifer for “revap” to occur (mm).	177.726
SOL_K	Saturated hydraulic conductivity.	−0.139
SOL_BD	Moist bulk density.	0.223
SOL_AWC	Available water capacity of the soil layer.	0.038
OV_N	Manning’s “n” value for overland flow.	−0.010
CANMX	Maximum canopy storage.	93.562
SLSUBBSN	Average slope length.	0.386
LAT_TTIME	Lateral flow travel time.	3.238
CNCOEF	Plant ET curve number coefficient.	0.678
CH_N2	Manning’s “n” value for the main channel.	0.023
CH_K2	Effective hydraulic conductivity in main channel alluvium.	65.951
HRU_SLP	Average slope steepness.	0.361

Furthermore, to study the impact of historical and projected climate conditions, two additional models for each watershed were developed for 45 years into the past and 45 years into the future, i.e., 1950–1994 and 2011–2055, respectively, with a warmup period of 1 year for each model. Development of the SWAT model for historical climate events requires historical weather data which were collected from Weather Data–NOAA Climate Data (1950–1994) (<https://swat.tamu.edu/data/>, accessed on 4 October 2022) [44] for both watersheds. Additionally, for the development of the SWAT model for projected climate events, the website of Coordinated Regional Climate Downscaling Experiment–North America (CORDEX–NA) (<https://na-cordex.org/>, accessed on 14 October 2022) [49], which archives Coupled Model Intercomparison Project phase 5 (CMIP5), was accessed and Representative Concentration Pathway 4.5 (RCP4.5) data from the EC–EARTH driver, Rossby Centre Regional Atmospheric Model version 4, (RCA4 model) were downloaded to collect daily precipitation, maximum air temperature, and minimum air temperature data. In this study, regional climatic model projected data and RCP4.5 (Representative Concentration Pathway 4.5) emission scenario were used. The regional climatic model generates high-resolution projections of future climate changes at a regional scale and RCP4.5 is considered the middle-of-the-road scenario, since it lies between lower-emissions

scenarios (RCP2.6 and RCP3-PD) and higher-emissions scenarios (RCP6 and RCP8.5). In the context of the United States, the projected mean temperature increases from 2 °C under the RCP 2.6 scenario to 5.5 °C under the RCP 8.5 scenario [49]. The regional climatic model at RCP4.5 does not estimate climate uncertainty but is used to drive climate models to produce projections of future climate change with more detailed information at a regional scale. The downloaded NetCDF formatted data were then downscaled by applying the linear scaling method in the climate model for hydrology (CMhyd) tool available on the SWAT website (<https://swat.tamu.edu/software/>, accessed on 20 January 2021) [50]. Historical data (1951–2005) and projected data (2006–2100) of 50 km spatial resolution were downloaded from CORDEX-NA and used with NOAA SWAT database’s observed data (1950–2010) for bias correction and data extraction in order to acquire data from 2011–2055 for the projected condition. A 90.2% overlap period was achieved with this approach, thus meeting the recommendation of the CMHyd tool [51]. The baseline model with fitted parameters was considered a control model, and the model developed based on historical and projected climate conditions was evaluated using the same set of parameters from the control model to detect the variation of flow in the past and the future. The flowchart of the methodology is shown in Figure 2.

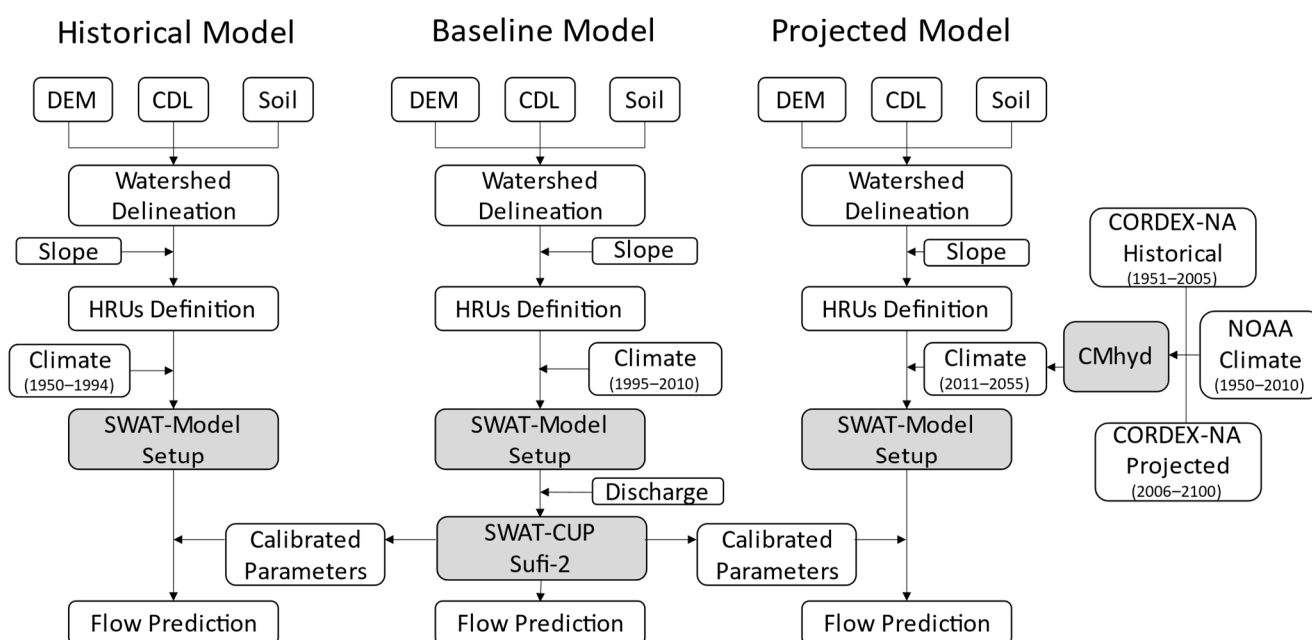


Figure 2. Flowchart of the methodology of SWAT model to study impact of climate change on flow. (DEM: Digital Elevation Model, CDL: Cropland Data Layer, HRU: Hydrologic Response Units, Coordinated Regional Climate Downscaling Experiment- North American, CMhyd: Climate Model data for hydrologic modeling, NOAA: National Oceanic and Atmospheric Administration, SWAT-CUP Sufi-2: SWAT Calibration and Uncertainty Programs Sequential Uncertainty Fitting version 2).

2.3. Model Evaluation

The simulation performance of the baseline models was evaluated using coefficient of determination (R^2) [52] (Equation (1)), Nash-Sutcliffe Efficiency (NSE) [53] (Equation (2)), Percentage Bias (PBAIS) [54] (Equation (3)), and KGE [48] (Equation (4)).

R^2 is the measure of model fit that shows the linear relation between observed and simulated data which ranges from 0 to 1. R^2 result approaching 1 indicates good model performance. NSE defines how well the observed and simulated data fits. NSE ranges from $-\infty$ to 1, 1 indicating a perfect fit. The average tendency of the simulated data to be greater or smaller than the observed data is measured by PBIAS. PBAIS negative value indicates overestimation and positive indicates underestimation. KGE is based on the decomposition

of the NSE and mean square error into correlation, bias error, variation coefficient error. KGE ranges between $-\infty$ to 1, where 1 is the optimal value.

$$R^2 = \left(\frac{\sum_{i=1}^N (O_i - \bar{O}) (S_i - \bar{S})}{\sqrt{\sum_{i=1}^N (O_i - \bar{O})^2} \cdot \sqrt{\sum_{i=1}^N (S_i - \bar{S})^2}} \right)^2 \quad (1)$$

$$NSE = 1 - \frac{\sum_{i=1}^N (O_i - S_i)^2}{\sum_{i=1}^N (O_i - \bar{O}_i)^2} \quad (2)$$

$$PBAIS = \frac{\sum_{i=1}^N (O_i - S_i)}{\sum_{i=1}^N O_i} \times 100 \quad (3)$$

where, O_i = observed value, \bar{O} = mean of observed values, S_i = simulated value, \bar{S} = mean of simulated values, and N = total number of observations [50–52].

And,

$$KGE = 1 - \sqrt{(r - 1)^2 + (\alpha - 1)^2 + (\beta - 1)^2} \quad (4)$$

where; r = Linear correlation coefficient between simulated and observed data; $\alpha = \frac{\sigma_s}{\sigma_o}$, a measure of relative variability of the predicted and observed runoff; σ_s and σ_o = Standard deviation of predicted and observed runoff; and β = Bias factor $\beta = \frac{\mu_s}{\mu_o}$; where μ is the mean of observed and simulated flows [48].

Moriasi et al. [55] hydrologic model calibration criteria for R^2 , NSE, and PBIAS were referred to determine the efficiency of the developed model, and Brighenti et al. [56] was referred for the evaluation criteria of KGE. After satisfactory calibration and validation of baseline model, the flow in the past (1951–1994 with one year warmup period) and in the future (2012–2055 with one year warmup period) were compared with respect to the baseline flow. Historical hydrological extreme events and future hydrological extreme events were also analyzed. Calibrated-validated period and onwards peak flow events of baseline model were considered for flood frequency analysis in this study.

2.4. Flood Frequency Analysis

The aim of analyzing the flood frequency was to use probability distribution to relate the magnitude of extreme flow events to the frequency of occurrence [57]. Log Pearson type III (LP3) distribution is recommended by USGS to fit extreme events for flood frequency analysis [58]. Generally, Annual Maximum Series (AMS) is considered as the flow extreme events for LP3 distribution. In this study, two different approaches were considered to identify extreme events. The first approach was to sort out AMS, and the second approach was to generate the Partial Duration Series (PDS) considering the 99th percentile ranked flow event during the respective period of different climatic conditions. These two data series of extreme events were fitted in LP3 distribution to generate flood frequency graphs. Detailed descriptions of the preparation of flood frequency curves using LP3 distribution can be found in Bulletin 17B guidelines (https://water.usgs.gov/osw/bulletin17b/dl_flow.pdf, accessed on 9 November 2022) [58].

3. Results

3.1. Streamflow Calibration and Validation

Figure 3 shows the trend of observed and simulated data for WRW monthly streamflow simulation after the model calibration and validation with SWAT-CUP. The R^2 ranged from 0.82 to 0.75 indicating good results, NSE ranged from 0.81 to 0.73 indicating very good to good results, PBAIS ranged from (−4.9) to (−3) indicating very good results and KGE ranged from 0.80 to 0.70 indicating good to intermediate results during model calibration and validation.

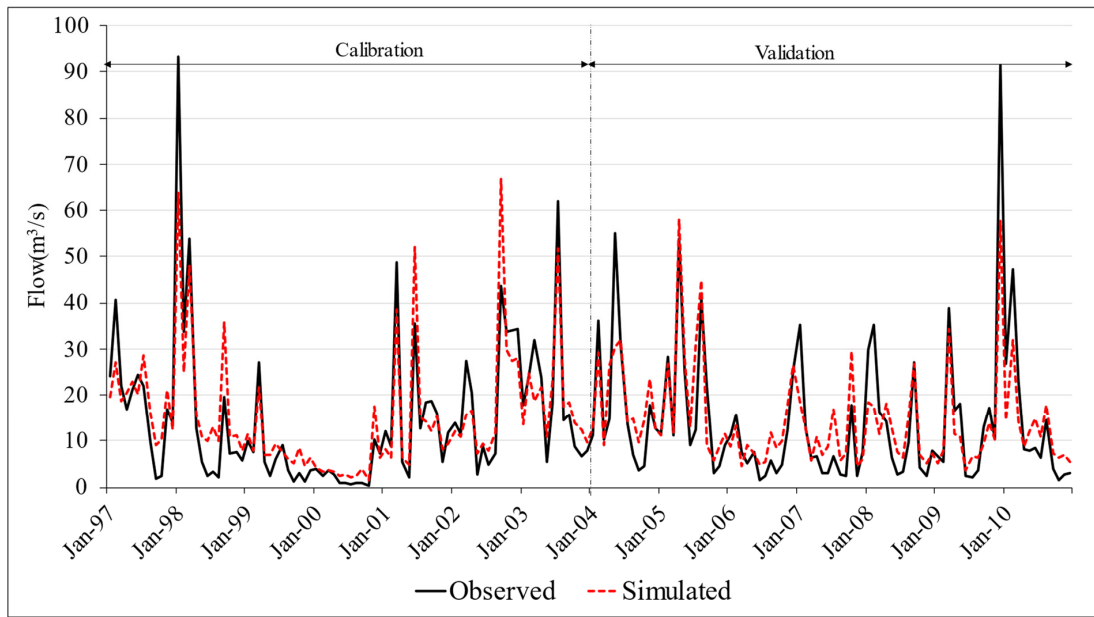


Figure 3. Monthly streamflow calibration-validation of Wolf River Watershed.

Similarly, Figure 4 shows the trend of observed and simulated data for JRW daily streamflow simulation after the model calibration and validation with SWAT-CUP. The R^2 ranged from 0.59 to 0.72 indicating not satisfactory to satisfactory results, NSE ranged from 0.42 to 0.71 indicating not satisfactory to good results, PBAIS ranged from 36.7 to 4.7 indicating not satisfactory to very good results whereas KGE ranged from 0.55 to 0.68 indicating intermediate results during model calibration-validation. Less than satisfactory results for R^2 , NSE, and PBAIS were observed. However, since KGE was defined as an objective function in calibration, the performance of the model was intermediate. Underestimation of the result might have occurred due to the lack of continuous observed streamflow data or due to the low-gradient topography of the JRW. The results of both model performances are summarized in Table 4.

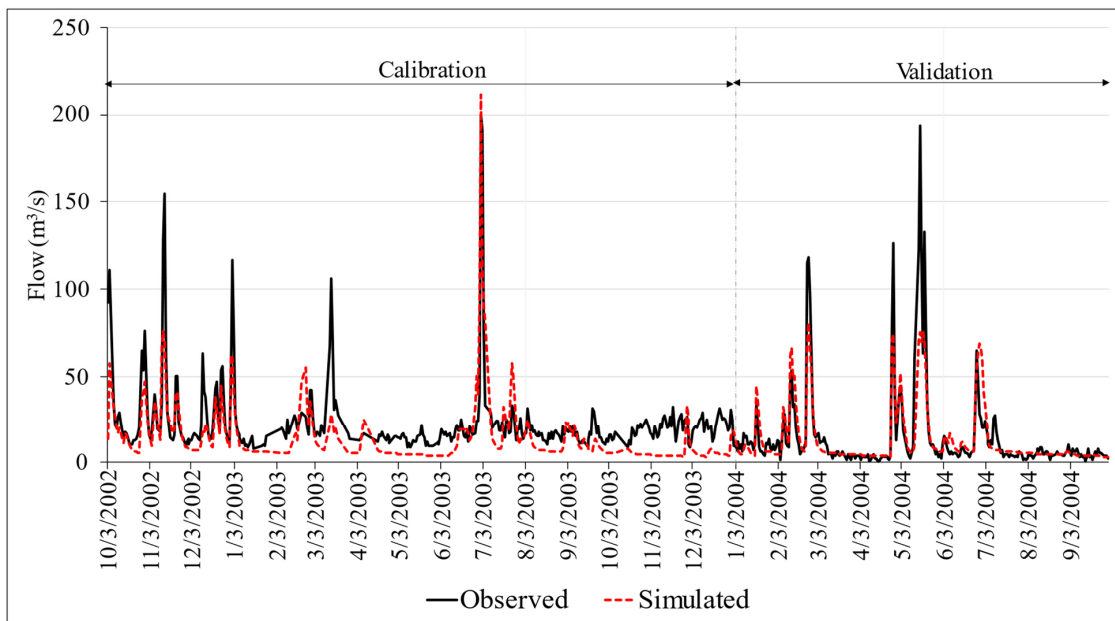


Figure 4. Daily streamflow calibration-validation of Jourdan River Watershed.

Table 4. Model performance of baseline SWAT model to simulate streamflow at Wolf River Watershed and Jourdan River Watershed.

Watershed	Model Development	R ²	NSE	PBIAS	KGE
WRW	Calibration (January 1997–December 2003)	0.82	0.81	−4.9	0.80
	Validation (January 2004–December 2010)	0.75	0.73	−3.0	0.70
JRW	Calibration (10 March 2002–31 December 2003)	0.59	0.42	36.7	0.55
	Validation (1 January 2004–30 September 2004)	0.72	0.71	4.7	0.68

3.2. Flow Comparison of Different Climate Conditions

The baseline average maximum temperature ($T_{max_{avg}}$) was 24.60 °C, the average minimum temperature ($T_{min_{avg}}$) was 13.67 °C and average precipitation (PPT_{avg}) was 3.77 mm for WRW. The acquired dataset shows that the historical $T_{max_{avg}}$ was 0.71 °C warmer and projected $T_{max_{avg}}$ will be 1.60 °C warmer as compared to the baseline condition. Whereas the historical $T_{min_{avg}}$ was 0.01 °C cooler and projected $T_{min_{avg}}$ will be 1 °C warmer than the baseline. Additionally, the historical PPT_{avg} was higher by 0.59 mm and projected PPT_{avg} will increase by 0.78 mm than the baseline condition. Although PPT_{avg} was higher in the historical condition, $Flow_{avg}$ was observed to be 0.14 mm less than baseline. Whereas, with increased PPT_{avg} in projected condition, the $Flow_{avg}$ was observed to increase by 1.23 mm in comparison to the baseline $Flow_{avg}$ of 13.89 mm.

Similarly, the baseline $T_{max_{avg}}$ was 24.54 °C, the $T_{min_{avg}}$ was 14.71 °C and PPT_{avg} was 3.90 mm for JRW. The historical $T_{max_{avg}}$ was 0.58 °C warmer and projected $T_{max_{avg}}$ will be 1.55 °C warmer compared to baseline. Whereas historical $T_{min_{avg}}$ was 0.46 °C cooler and projected $T_{min_{avg}}$ will be 0.65 °C warmer than the baseline. Moreover, the historical PPT_{avg} was 0.51 mm higher and projected PPT_{avg} will be 0.77 mm higher than the baseline. Due to the increase in PPT_{avg} in both climatic conditions, the increase in flow was observed in both climates in JRW. The predicted historical $Flow_{avg}$ was observed to be 1.25 mm high and projected $Flow_{avg}$ was observed to increase by 0.65 mm as compared to the baseline $Flow_{avg}$ of 11.47 mm.

The trend of streamflow obtained by plotting the monthly averaged flow of SWAT flow output from the historical and projected models, presented in Figures 5 and 6, was analyzed with respect to the baseline model. In the context of WRW, there was an increment during spring and a reduction during fall in both climatic conditions, whereas during summer, the projected streamflow appeared larger than the historical and, in most cases, exceeded the baseline, too. Historical flow exceeded the baseline flow in 6 months and was lower than that in 6 months (Dec–May), whereas projected flow exceeded the baseline flow in 7 months (Jan–May and July–Aug) and was lower than that in 5 months (Jun and Sep–Dec). Overall, with respect to the baseline monthly average of streamflow, a reduction in the historical flow and an increment in the projected flow were estimated in WRW.

In the context of JRW, there too was an increment during spring and a reduction during fall in both climatic conditions, whereas in summer, the projected streamflow appeared higher in July–August and historical appeared higher in May. However, in the rest of the cases, both conditions' streamflow was lower than that of the baseline. Historical flow exceeded the baseline flow in 6 months and was lower in 6 months (Jan–May and Aug), whereas projected flow exceeded the baseline flow in 7 months (Jan–Mar and May–Aug) and was lower in 5 months (April and Sep–Dec). Overall, with respect to the baseline monthly averaged stream flow, increments in both historical and projected flow were estimated in JRW.

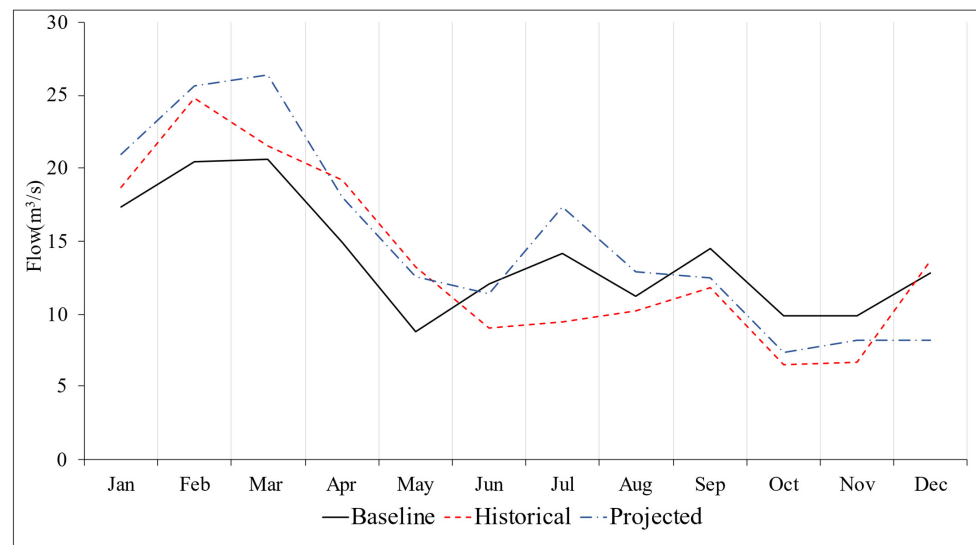


Figure 5. Monthly averaged streamflow flow comparison of Wolf River Watershed. (Historical: 1951–1994, Baseline: 1997–2010, Projected: 2012–2055).

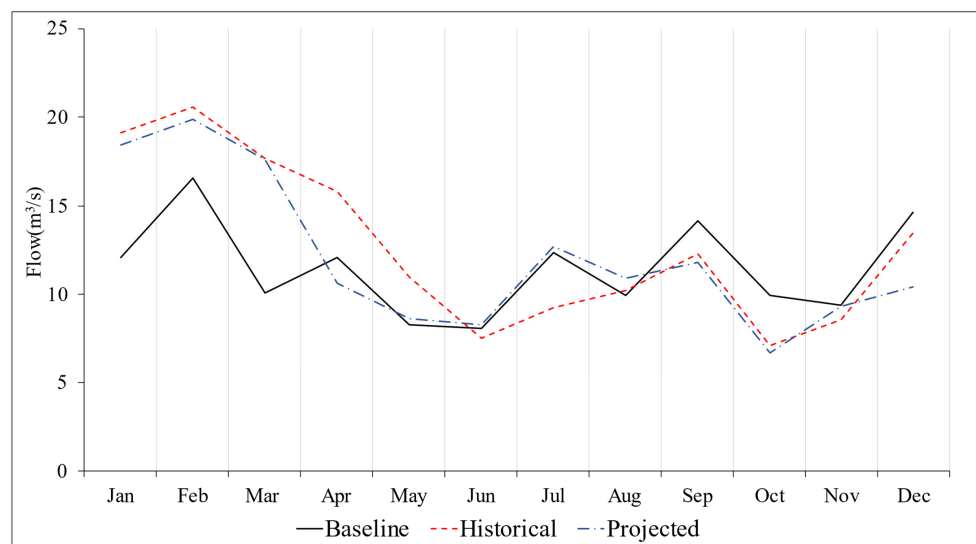


Figure 6. Monthly averaged streamflow flow comparison of Jourdan River Watershed. (Historical: 1951–1994, Baseline: 1997–2010, Projected: 2012–2055).

3.3. Flow Extreme Events

Annual maximum peak flow series: The maximum flow events of each year from all climatic conditions were sorted to produce AMS, as shown in Figure 7. In total, 14 peaks from baseline (1997–2010) and 44 peaks each from historical (1951–1994) and projected (2012–2055) conditions were captured to obtain AMS for WRW. Similarly, for JRW, 9 peaks from baseline (2002–2010) and 44 peaks each from historical (1951–1994) and projected (2012–2055) conditions were captured to obtain AMS.

Partial duration peak flow series: Partial duration peak flow series for every condition in this study was obtained by defining the 99th percentile ranking; it is plotted in Figure 8. For WRW, 52 peak flow events in 14 years of the baseline condition, 161 peak flow events in 44 years of the historical climatic condition, and 161 peak flow events in 44 years of the projected climatic condition were defined as extreme values for the streamflow. Similarly, 33 peak flow events in 8 years of the baseline condition, 161 peak flow events in 44 years of the historical climatic condition, and 161 peak flow events in 44 years of the projected climatic condition were identified in JRW.

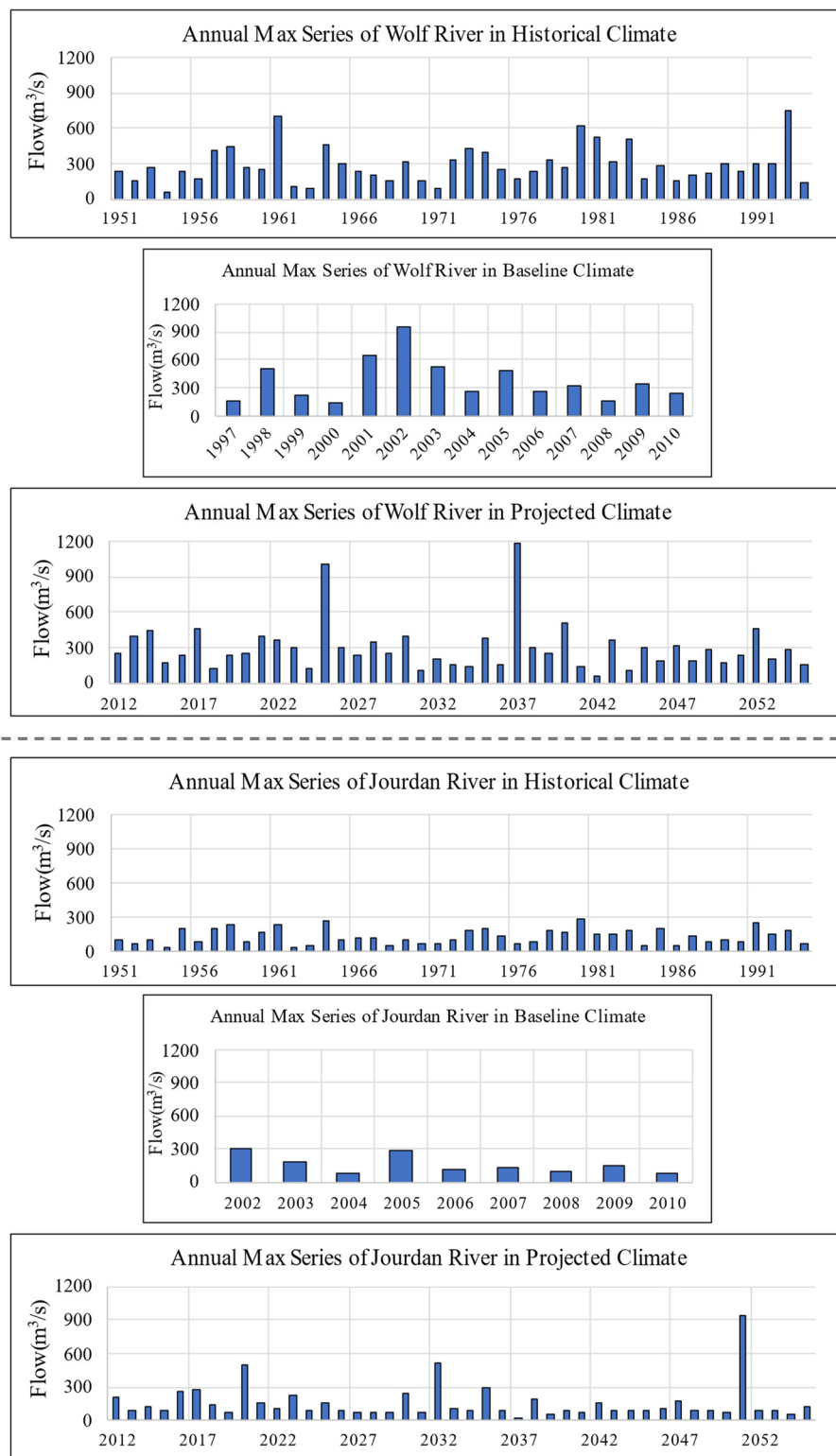


Figure 7. Annual maximum series graph for different climatic conditions.

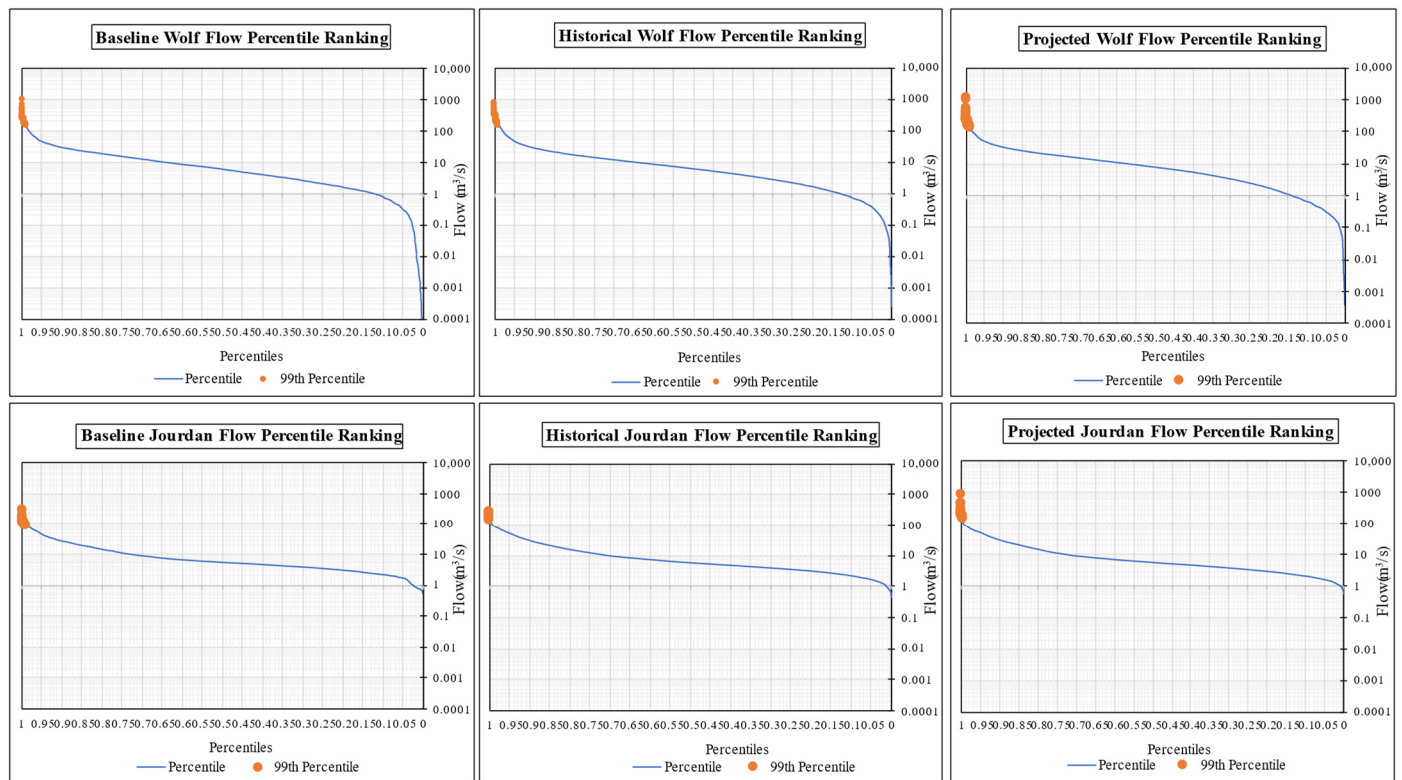


Figure 8. 99th percentile ranking of streamflow at different climatic conditions.

The gamma distribution plot using the shape–scale parameterization for 99th percentile peak flow PDS is shown in Figure 9. The plot shows the relation between peak flows and its probability of occurrence. The probability of occurrence was highest during the historical condition in both WRW and JRW, whereas the probability of occurrence was the lowest for the baseline PDS in WRW and projected PDS for JRW. Since the highest amongst the lowest flow magnitude in all climatic condition PDS of WRW was $146.7 \text{ m}^3/\text{s}$ in historical PDS, the graph was plotted from $150 \text{ m}^3/\text{s}$ through $1200 \text{ m}^3/\text{s}$ to include $1185 \text{ m}^3/\text{s}$ flow of highest right-skewed projected PDS in Figure 9a. Similarly for JRW, the highest PDS amongst the lowest flow magnitude in all climatic conditions was $92.17 \text{ m}^3/\text{s}$. Therefore, Figure 9b was plotted from $100 \text{ m}^3/\text{s}$ to $1000 \text{ m}^3/\text{s}$ in order to include $934.4 \text{ m}^3/\text{s}$ highest right-skewed projected PDS. From this distribution, the largest magnitude of the flow extreme series was predicted during the projected condition for both watersheds.

3.4. Flood Frequency Analysis

The flood frequency analysis was carried out with Log Pearson type III (LP3) distribution graph using AMS and PDS as shown in Figures 10 and 11 for WRW and JRW, respectively. A spreadsheet model was developed to compute the exceedance probability and to plot flood frequency curve using LP3 distribution. Pearson type III deviation was calculated using standard normal deviation and a skewness coefficient of the logarithm of peak flow [58]. The 95% confidence interval capturing the uncertainty in the estimate of flood probabilities of the extreme flow events is also shown in Figures 10 and 11. Lower and upper bound curves are generated using a probability coefficient with a 95% confidence interval based on the peak flow records. Plotting the extreme flow values against the exceedance probability using standardized methods such as LP3 distribution can be used to extrapolate flooding events beyond the experienced values [58].

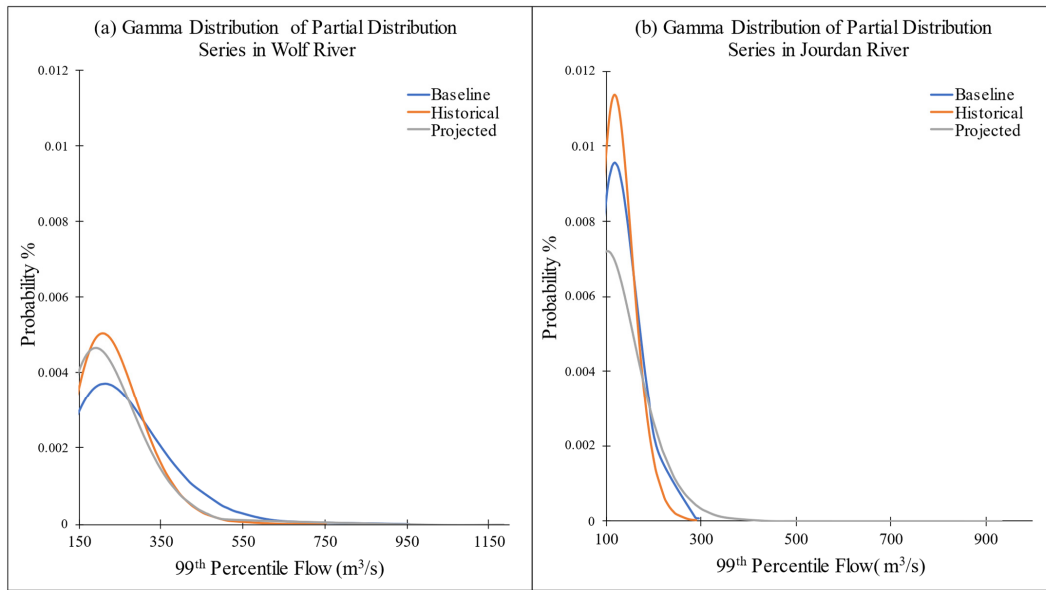


Figure 9. (a,b) Gamma distribution plot of partial distribution series.

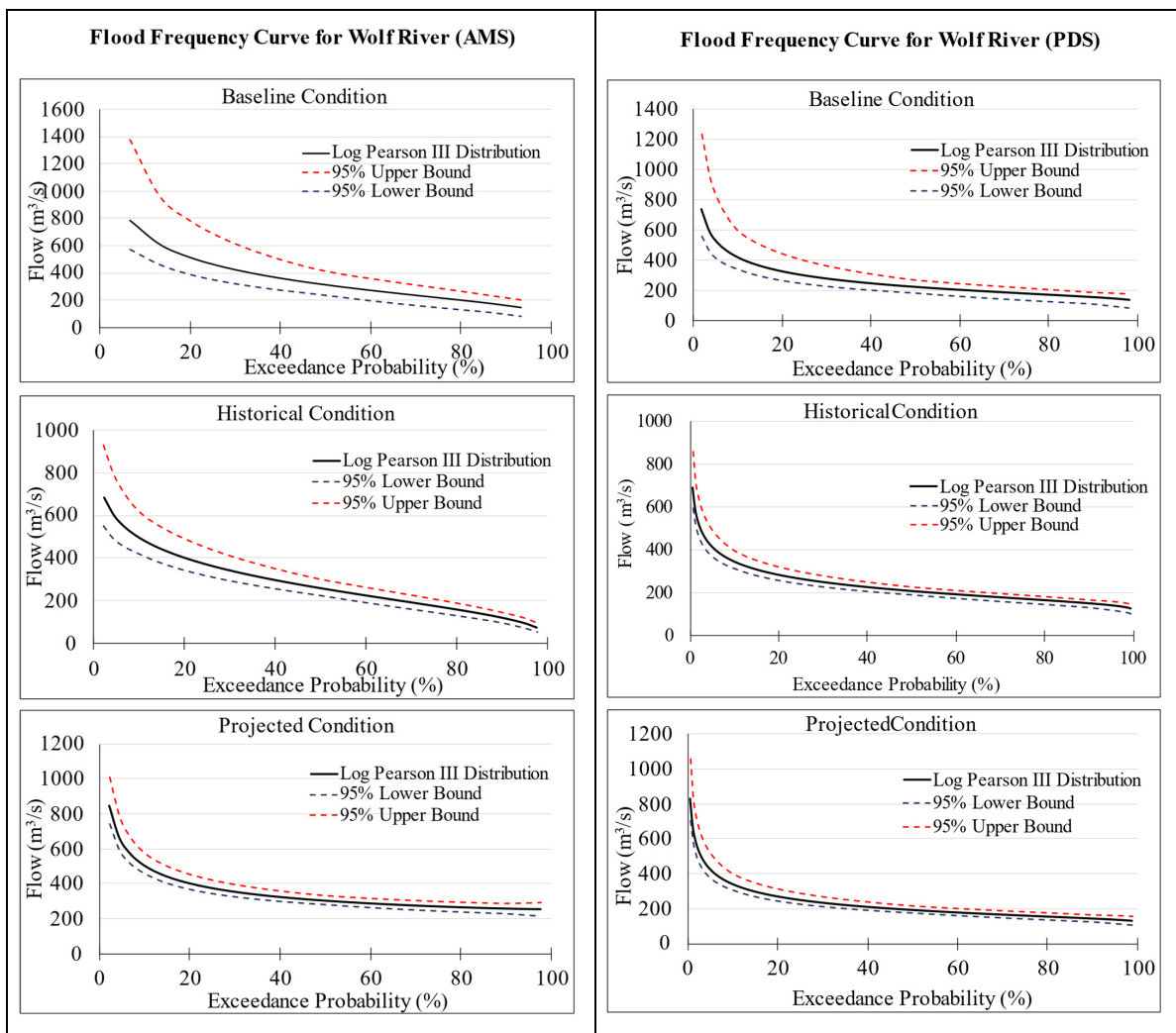


Figure 10. Wolf River flood frequency curves for the annual maximum series and partial duration series.

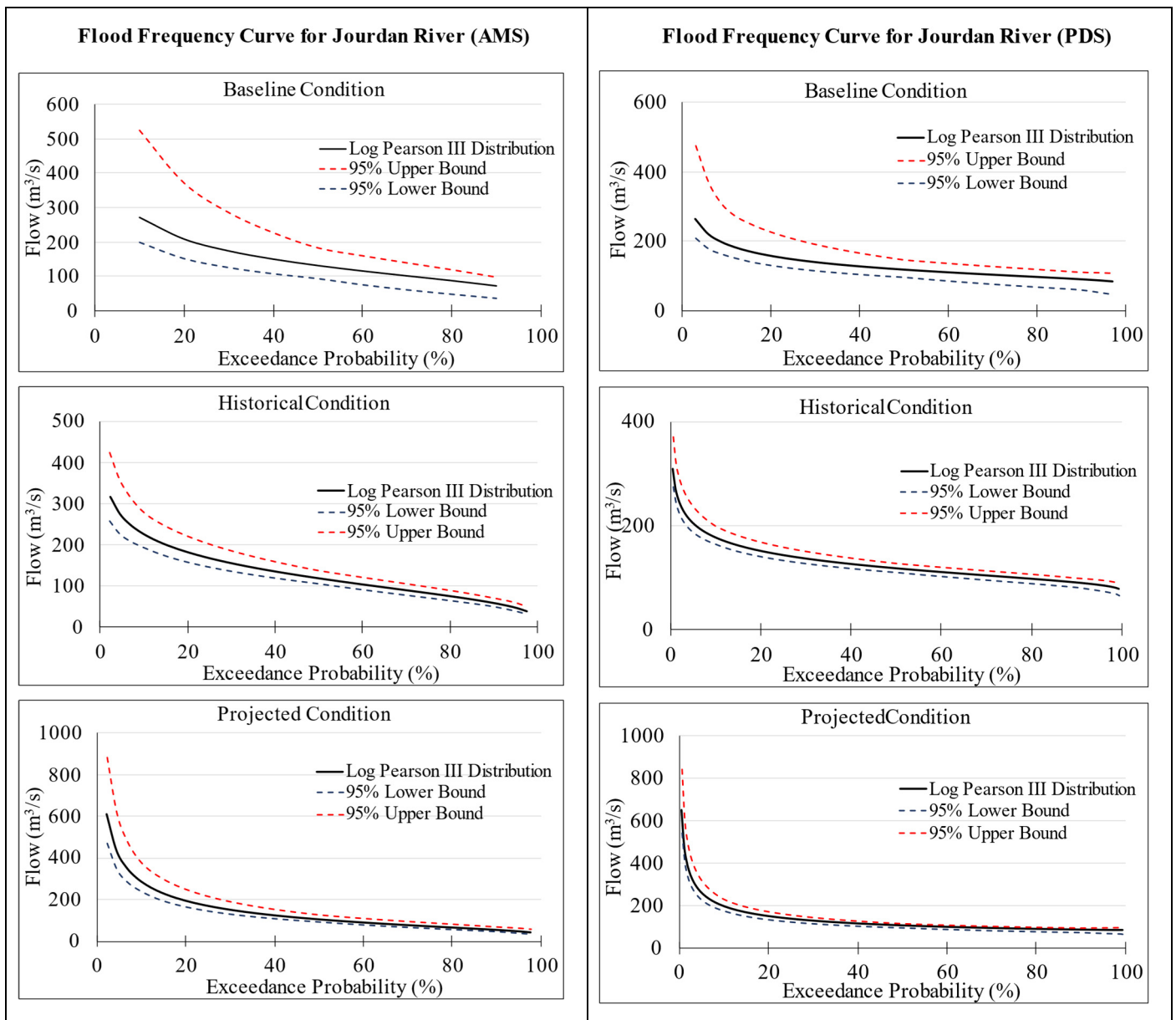


Figure 11. Jourdan River flood frequency curves for the annual maximum series and partial duration series.

In Figures 12 and 13, both AMS and PDS are plotted together to compare the flood frequency curve at different climatic conditions using different peak flow series. Comparing Figures 12 and 13, the peak flow estimated by the AMS series is higher than the one estimated by the PDS series in both watersheds. While comparing the 1% exceedance probability, i.e., 100-year return flood, it increased by 27% from historical to baseline condition with AMS but decreased by 22% from baseline to projected condition in WRW. Similarly, with PDS, the 1% exceedance probability increased by 17% from historical to baseline, and decreased again by 15% from baseline to projected condition.

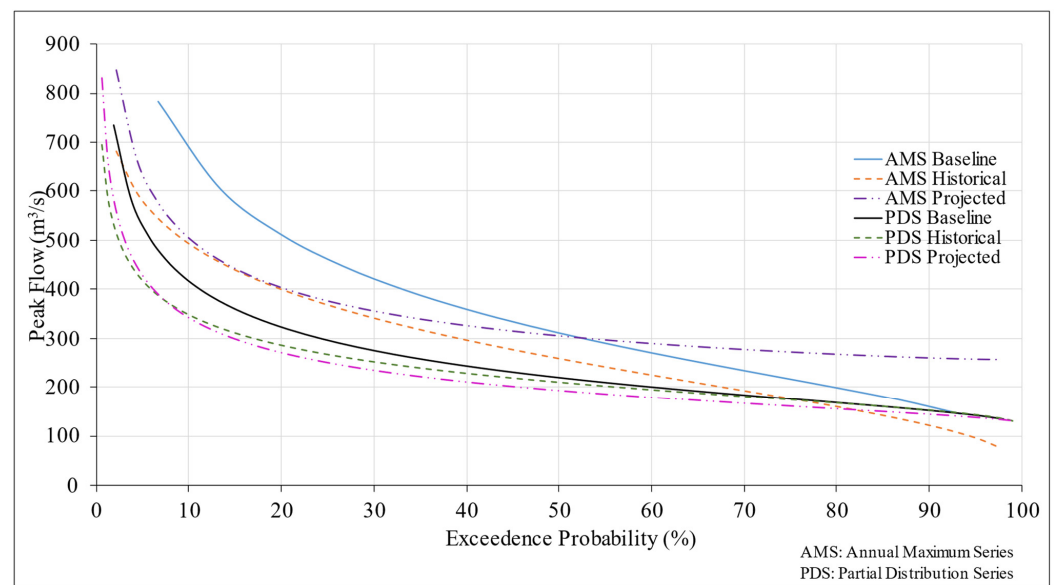


Figure 12. Wolf River Flood frequency curve at different climatic conditions with different peak flow series.

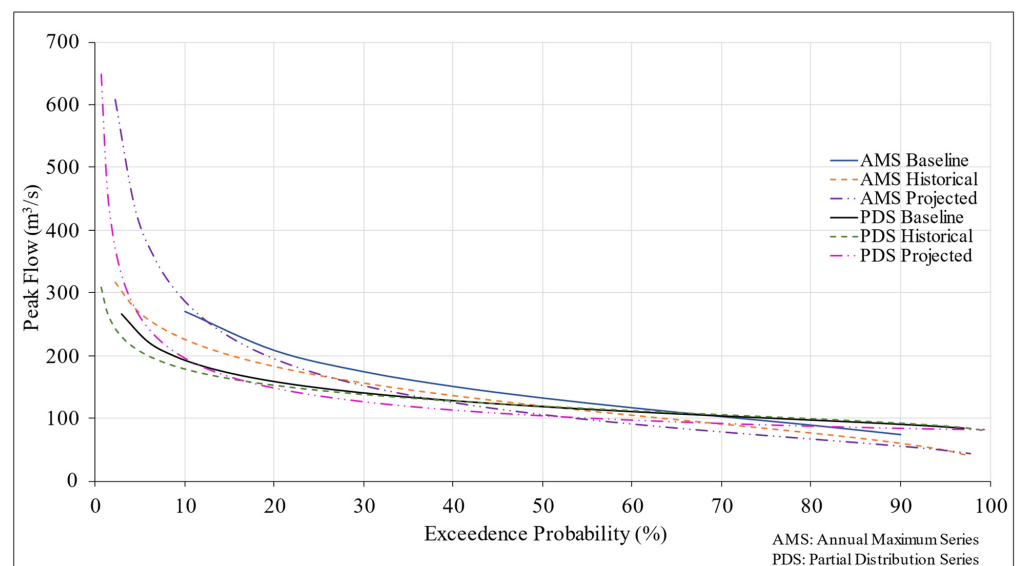


Figure 13. Jourdan River flood frequency curve at different climatic conditions with different peak flow series.

In JRW, the 1% exceedance probability increased by 8.1% from historical to baseline and further increased by 17% from baseline to projected with AMS. Similarly, with PDS, the 1% exceedance probability increased from 4.4% from historical to baseline and 10% from baseline to projected condition.

4. Discussion

This study aims to investigate the impact of climate change on the streamflow from the coastal watersheds of Mississippi draining into the Saint Louis Bay by comparing historical and projected climate events. The findings on the model development, and the calibration–validation process suggest that the SWAT model is capable of simulating the hydrological phenomenon in the forested coastal watershed as described by Upadhyay et al. [35]. Moreover, the results of statistical measures were considerably better in the watershed with continuous discharge data. Both models were able to generate satisfactory KGE values, indicating the reliability of the model performance [56]. The

comparison of flow between different climatic conditions depicted an increment of monthly averaged flow in comparison to the baseline and historical climate. This might have been a result of the increased precipitation in the coastal watershed of Mississippi as mentioned in Sankar et al.'s [39] and Parra et al.'s [40] works. Since IPCC [5] highlights the risk of extreme precipitation and flooding in coastal regions due to climate change, riverine flooding risk was also analyzed in this study. Flood frequency analysis using LP3 distribution revealed that the 1% exceedance probability was highest in the AMS of the baseline condition in WRW, whereas for JRW, the AMS of the projected condition was highest. The increment in exceedance probability in the future condition in JRW aligns with the recent study carried out on the coastal plain of northeastern United States [59]. Contrary to JRW, the 1% exceedance probability is the highest in the baseline condition of WRW. Although both watersheds are adjacent to each other, the flood frequency at the outlet of these watersheds varies significantly given the same future climate condition. In addition, during the flood frequency analysis of JRW, we used the AMS baseline condition with only nine years for peak flow data. Therefore, in the estimation of 1% exceedance probability, there are higher uncertainties.

Since flood frequency analysis can predict the likelihood of flood occurrence, flood warning systems and emergency response plans for vulnerable areas can be developed beforehand. Infrastructure design and construction could consider the magnitude and frequency of predicted flooding events in order to minimize the unforeseeable damage to life and property.

5. Conclusions

This study compared the variation in flow in different climates and analyzed the flood frequencies in the two forest-dominated coastal watersheds, WRW and JRW. Baseline models for two adjacent coastal watersheds were developed using the SWAT model and auto-calibrated with the SWATCUP-Sufi2 tool applying KGE as an objective function. The fitted parameters used to develop an acceptable baseline model were further used to set up different climatic models to study the impact of climate change on the streamflow of both watersheds in different periods. The historical climatic model was developed using observed weather data from NOAA, and for the development of the projected climatic model, the CMIP5 CORDEX-NA data were downloaded and downscaled using the CMhyd tool to acquire projected weather data. The streamflow during different climatic conditions in the past and the future was compared with the baseline streamflow and the variation in the magnitude was analyzed. Log Pearson type III distribution was used to fit the AMS and PDS to analyze the flood frequency of the stream at different climatic conditions extremities. This study quantifies the hydrologic response of Wolf River Watershed and Jourdan River Watershed due to historical and future projected climatic conditions, which aids in the management of future flooding.

Author Contributions: S.B.: conceptualization, data curation, formal analysis, methodology, software, visualization, writing—original draft. P.B.P.: conceptualization, funding acquisition, methodology, resources, supervision, validation, writing—review and editing. F.T.: writing—review and editing. All authors have read and agreed to the published version of the manuscript.

Funding: This project was paid for in part with federal funding from the U.S. Department of the Treasury, the Mississippi Department of Environmental Quality, and the Mississippi Based RESTORE Act Center of Excellence under the Resources and Ecosystems Sustainability, Tourist Opportunities, and Revived Economies of the Gulf Coast States Act of 2012 (RESTORE Act). The statements, findings, conclusions, and recommendations are those of the authors and do not necessarily reflect the views of the Department of the Treasury, the Mississippi Department of Environmental Quality, or the Mississippi Based RESTORE Act Center of Excellence.

Institutional Review Board Statement: Not applicable.

Informed Consent Statement: Not applicable.

Data Availability Statement: Not applicable.

Acknowledgments: We would like to acknowledge the partial support of the Bagley College of Engineering, Mississippi Agricultural and Forestry Experiment Services (MAFES), and College of Agriculture and Life Sciences at Mississippi State University, United States Geological Survey (USGS), and all our collaborators in this study.

Conflicts of Interest: The authors declare no conflict of interest.

References

- Pörtner, H.O. (Ed.) *Climate Change 2022: Impacts, Adaptation and Vulnerability Working Group II Contribution to the Sixth Assessment Report of the Intergovernmental Panel on Climate Change*; Cambridge University Press: Cambridge, UK, 2022. [CrossRef]
- Lee, C.H.; Yeh, H.F. Impact of Climate Change and Human Activities on Streamflow Variations Based on the Budyko Framework. *Water* **2019**, *11*, 2001. [CrossRef]
- Chiang, L.C.; Liao, C.J.; Lu, C.M.; Wang, Y.C. Applicability of Modified SWAT Model (SWAT-Twn) on Simulation of Watershed Sediment Yields under Different Land Use/Cover Scenarios in Taiwan. *Environ. Monit. Assess.* **2021**, *193*, 1–23. [CrossRef] [PubMed]
- Giorgi, F.; Raffaele, F.; Coppola, E. The Response of Precipitation Characteristics to Global Warming from Climate Projections. *Earth Syst. Dyn.* **2019**, *10*, 73–89. [CrossRef]
- Pachauri, R.K.; Allen, M.R.; Barros, V.R.; Broome, J.; Cramer, W.; Christ, R.; Church, J.A.; Clarke, L.; Dahe, Q.; Dasgupta, P.; et al. *Climate Change 2014: Synthesis Report; Contribution of Working Groups I, II and III to the Fifth Assessment Report of the Intergovernmental Panel on Climate Change*; IPCC: Geneva, Switzerland, 2014; p. 151.
- Merkens, J.L.; Reimann, L.; Hinkel, J.; Vafeidis, A.T. Gridded Population Projections for the Coastal Zone under the Shared Socioeconomic Pathways. *Glob. Planet. Change* **2016**, *145*, 57–66. [CrossRef]
- Kron, W. Coasts: The High-Risk Areas of the World. *Nat. Hazards* **2013**, *66*, 1363–1382. [CrossRef]
- Boithias, L.; Sauvage, S.; Lenica, A.; Roux, H.; Abbaspour, K.C.; Larnier, K.; Dartus, D.; Sánchez-Pérez, J.M. Simulating Flash Floods at Hourly Time-Step Using the SWAT Model. *Water* **2017**, *9*, 929. [CrossRef]
- Zhang, K.; Shalehy, M.H.; Ezaz, G.T.; Chakraborty, A.; Mohib, K.M.; Liu, L. An Integrated Flood Risk Assessment Approach Based on Coupled Hydrological-Hydraulic Modeling and Bottom-up Hazard Vulnerability Analysis. *Environ. Model. Softw.* **2022**, *148*, 105279. [CrossRef]
- Chao, L.; Zhang, K.; Li, Z.; Wang, J.; Yao, C.; Li, Q. Applicability Assessment of the CASCade Two Dimensional SEDiment (CASC2D-SED) Distributed Hydrological Model for Flood Forecasting across Four Typical Medium and Small Watersheds in China. *J. Flood Risk Manag.* **2019**, *12*, e12518. [CrossRef]
- Jodar-Abellan, A.; Valdes-Abellan, J.; Pla, C.; Gomariz-Castillo, F. Impact of Land Use Changes on Flash Flood Prediction Using a Sub-Daily SWAT Model in Five Mediterranean Ungauged Watersheds (SE Spain). *Sci. Total Environ.* **2019**, *657*, 1578–1591. [CrossRef]
- Li, W.; Lin, K.; Zhao, T.; Lan, T.; Chen, X.; Du, H.; Chen, H. Risk Assessment and Sensitivity Analysis of Flash Floods in Ungauged Basins Using Coupled Hydrologic and Hydrodynamic Models. *J. Hydrol.* **2019**, *572*, 108–120. [CrossRef]
- Nkwunonwo, U.C.; Whitworth, M.; Baily, B. A Review of the Current Status of Flood Modelling for Urban Flood Risk Management in the Developing Countries. *Sci. Afr.* **2020**, *7*, e00269. [CrossRef]
- Arnold, J.G.; Srinivasan, R.; Muttiah, R.S.; Williams, J.R. Large Area Hydrologic Modeling and Assessment Part I: Model Development 1. *J. Am. Water Resour. Assoc.* **1998**, *34*, 73–89. [CrossRef]
- Roux, H.; Labat, D.; Garambois, P.A.; Maubourguet, M.M.; Chorda, J.; Dartus, D. A Physically-Based Parsimonious Hydrological Model for Flash Floods in Mediterranean Catchments. *Nat. Hazards Earth Syst. Sci.* **2011**, *11*, 2567–2582. [CrossRef]
- Brunner, G.W. HEC-RAS River Analysis System. Hydraulic Reference Manual. Version 1.0. Hydrologic Engineering Center Davis CA. 1995. Available online: <https://www.hec.usace.army.mil/confluence/rasdocs/ras1dtechref/latest> (accessed on 2 December 2022).
- Kastridis, A.; Stathis, D. Evaluation of Hydrological and Hydraulic Models Applied in Typical Mediterranean Ungauged Watersheds Using Post-Flash-Flood Measurements. *Hydrology* **2020**, *7*, 12. [CrossRef]
- Feldman, A.D. *Hydrologic Modeling System HEC-HMS Technical Reference Manual*; US Army Corps of Engineers, Hydrologic Engineering Center: Davis, CA, USA, 2000.
- Julien, P.Y.; Saghafian, B. CASC2D User's Manual: A Two-Dimensional Watershed Rainfall-Runoff Model; Diss. Colorado State University. *Libraries* **1991**, 1–66.
- Beven, K.J.; Kirkby, M.J. A Physically Based, Variable Contributing Area Model of Basin Hydrology. *Hydrol. Sci. J.* **1979**, *24*, 43–69. [CrossRef]
- MIKE FLOOD 1D-2D and 1D-3D Modelling User Manual. *DHI Water Environ.* **2021**, 1–154.
- Ajmal, A.; Irfan, S.; Sabahat, N.; Saleem, S.B. Analysis of Flood Risk Management in the Context of Mathematical Models. In Proceedings of the 2019 International Conference on Innovative Computing (ICIC)2019, Lahore, Pakistan, 1–2 November 2019; pp. 1–6. [CrossRef]

23. Iqbal, M.S.; Dahri, Z.H.; Querner, E.P.; Khan, A.; Hofstra, N. Impact of Climate Change on Flood Frequency and Intensity in the Kabul River Basin. *Geosciences* **2018**, *8*, 114. [CrossRef]
24. Khan, S.I.; Hong, Y.; Wang, J.; Yilmaz, K.K.; Gourley, J.J.; Adler, R.F.; Brakenridge, G.R.; Policelli, F.; Habib, S.; Irwin, D. Satellite Remote Sensing and Hydrologic Modeling for Flood Inundation Mapping in Lake Victoria Basin: Implications for Hydrologic Prediction in Ungauged Basins. *IEEE Trans. Geosci. Remote Sens.* **2010**, *49*, 85–95. [CrossRef]
25. SWAT Literature Database for Peer-Reviewed Journal Articles. Center for Agricultural and Rural Development, Ames, IA, USA. 2022. Available online: https://www.card.iastate.edu/swat_articles/ (accessed on 1 December 2022).
26. Parajuli, P.B.; Risal, A. Evaluation of Climate Change on Streamflow, Sediment, and Nutrient Load at Watershed Scale. *Climate* **2021**, *9*, 165. [CrossRef]
27. Bhatta, B.; Shrestha, S.; Shrestha, P.K.; Talchabhadel, R. Evaluation and Application of a SWAT Model to Assess the Climate Change Impact on the Hydrology of the Himalayan River Basin. *Catena* **2019**, *181*, 104082. [CrossRef]
28. Kiesel, J.; Gericke, A.; Rathjens, H.; Wetzig, A.; Kakouei, K.; Jähnig, S.C.; Fohrer, N. Climate Change Impacts on Ecologically Relevant Hydrological Indicators in Three Catchments in Three European Ecoregions. *Ecol. Eng.* **2019**, *127*, 404–416. [CrossRef]
29. Nguyen, H.H.; Recknagel, F.; Meyer, W.; Frizenschaf, J.; Shrestha, M.K. Modelling the Impacts of Altered Management Practices, Land Use and Climate Changes on the Water Quality of the Millbrook Catchment-Reservoir System in South Australia. *J. Environ. Manag.* **2017**, *202*, 1–11. [CrossRef] [PubMed]
30. Rabezanahary Tantelinaiaina, M.F.; Rahaman, M.H.; Zhai, J. Assessment of the Future Impact of Climate Change on the Hydrology of the Mangoky River, Madagascar Using ANN and SWAT. *Water* **2021**, *13*, 1239. [CrossRef]
31. Singh, V.; Sharma, A.; Goyal, M.K. Projection of Hydro-Climatological Changes over Eastern Himalayan Catchment by the Evaluation of RegCM4 RCM and CMIP5 GCM Models. *Hydrol. Res.* **2019**, *50*, 117–137. [CrossRef]
32. Menna, B.Y. Simulation of Hydro Climatological Impacts Caused by Climate Change: The Case of Hare Watershed, Southern Rift Valley of Ethiopia. *Hydrol Curr. Res.* **2017**, *8*, 2. [CrossRef]
33. Devkota, L.P.; Gyawali, D.R. Impacts of Climate Change on Hydrological Regime and Water Resources Management of the Koshi River Basin, Nepal. *J. Hydrol. Reg. Stud.* **2015**, *4*, 502–515. [CrossRef]
34. Maghsood, F.F.; Moradi, H.; Massah Bavani, A.R.; Panahi, M.; Berndtsson, R.; Hashemi, H. Climate Change Impact on Flood Frequency and Source Area in Northern Iran under CMIP5 Scenarios. *Water* **2019**, *11*, 273. [CrossRef]
35. Upadhyay, P.; Linhoss, A.; Kelble, C.; Ashby, S.; Murphy, N.; Parajuli, P.B. Applications of the SWAT Model for Coastal Watersheds: Review and Recommendations. *J. ASABE* **2022**, *65*, 453–469. [CrossRef]
36. Kundzewicz, Z.W. Climate Change Impacts on the Hydrological Cycle. *Ecohydrol. Hydrobiol.* **2008**, *8*, 195–203. [CrossRef]
37. Wuebbles, D.; Fahey, D.; Takle, E.; Hibbard, K.; Arnold, J.; DeAngelo, B.; Doherty, S.; Easterling, D.; Edmonds, J.; Edmonds, T.; et al. *Climate Science Special Report: Fourth National Climate Assessment (NCA4), Volume I*; U.S. Global Change Research Program: Washington, DC, USA, 2017.
38. Kunkel, K.E.; Frankson, R.; Runkle, J.; Champion, S.M.; Stevens, L.E.; Easterling, D.R.; Stewart, B.C.; McCarrick, A.; Lemery, C.R. State Climate Summaries for the United States 2022. NOAA Technical Report NESDIS 150. NOAA NESDIS. 2022. Available online: <https://www.nesdis.noaa.gov/about/documents-reports/technical-reports> (accessed on 4 October 2022).
39. Sankar, M.S.; Dash, P.; Lu, Y.; Hu, X.; Mercer, A.E.; Wickramarathna, S.; Beshah, W.T.; Sanders, L.; Arslan, Z.; Dyer, J.; et al. Seasonal Changes of Trace Metal-Nutrient-Dissolved Organic Matter Conveyance along with Coastal Acidification over the Largest Oyster Reef in Western Mississippi Sound, Northern Gulf of Mexico. *North. Gulf Mex.* **2021**. [CrossRef]
40. Parra, S.M.; Sanial, V.; Boyette, A.D.; Cambazoglu, M.K.; Soto, I.M.; Greer, A.T.; Chiaverano, L.M.; Hoover, A.; Dinniman, M.S. Bonnet Carré Spillway Freshwater Transport and Corresponding Biochemical Properties in the Mississippi Bight. *Cont. Shelf Res.* **2020**, *199*, 104114. [CrossRef]
41. Dile, Y.T.; Daggupati, P.; George, C.; Srinivasan, R.; Arnold, J. Introducing a New Open Source GIS User Interface for the SWAT Model. *Environ. Model. Softw.* **2016**, *85*, 129–138. [CrossRef]
42. Neitsch, S.L.; Arnold, J.G.; Kiniry, J.R.; Srinivasan, R.; Williams, J.R. *Soil and Water Assessment Tool User's Manual, Version 2000*; Texas Water Resources Institute: College Station, TX, USA, 2000; pp. 1–27.
43. USGS The National Map-Advanced Viewer. Available online: <https://apps.nationalmap.gov/viewer/> (accessed on 4 October 2022).
44. Global Data | SWAT | Soil & Water Assessment Tool. Available online: <https://swat.tamu.edu/data/> (accessed on 4 October 2022).
45. CropScape-NASS CDL Program. Available online: <https://nassgeodata.gmu.edu/CropScape/> (accessed on 4 October 2022).
46. Abbaspour, K.C. *Swat-Cup 2012. SWAT Calibration and Uncertainty Program—A User Manual*; Swiss Federal Institute of Aquatic Science and Technology: Dübendorf, Switzerland, 2013.
47. Sao, D.; Kato, T.; Tu, L.H.; Thouk, P.; Fitriyah, A.; Oeurng, C. Evaluation of Different Objective Functions Used in the SUFI-2 Calibration Process of SWAT-CUP on Water Balance Analysis: A Case Study of the Pursat River Basin, Cambodia. *Water* **2020**, *12*, 2901. [CrossRef]
48. Gupta, H.V.; Kling, H.; Yilmaz, K.K.; Martinez, G.F. Decomposition of the Mean Squared Error and NSE Performance Criteria: Implications for Improving Hydrological Modelling. *J. Hydrol.* **2009**, *377*, 80–91. [CrossRef]
49. Mearns, L.; McGinnis, S.; Korytina, D.; Arritt, R.; Biner, S.; Bukovsky, M.; Chang, H.; Christensen, O.; Herzmann, D.; Jiao, Y.; et al. 2017: The NA-CORDEX Dataset, Version 1.0. NCAR Climate Data Gateway, Boulder CO. 2017. Available online: <https://na-cordex.org/> (accessed on 14 October 2022). [CrossRef]

50. Software | SWAT | Soil & Water Assessment Tool. Available online: <https://swat.tamu.edu/software/> (accessed on 20 January 2021).
51. Rathjens, H.; Bieger, K.; Srinivasan, R.; Chaubey, I.; Arnold, J.G. CMhyd User Manual Documentation for Preparing Simulated Climate Change Data for Hydrologic Impact Studies. 2016. Available online: <http://swat.tamu.edu/software/cmhyd> (accessed on 15 October 2022).
52. Krause, P.; Boyle, D.P.; Båse, F. Comparison of Different Efficiency Criteria for Hydrological Model Assessment. *Adv. Geosci.* **2005**, *5*, 89–97. [[CrossRef](#)]
53. Nash, J.E.; Sutcliffe, J.V. River Flow Forecasting through Conceptual Models Part I-A Discussion of Principles. *J. Hydrol.* **1970**, *10*, 282–290. [[CrossRef](#)]
54. Gupta, H.V.; Sorooshian, S.; Yapo, P.O. Status of Automatic Calibration for Hydrologic Models: Comparison with Multilevel Expert Calibration. *J. Hydrol. Eng.* **1999**, *4*, 135–143. [[CrossRef](#)]
55. Moriasi, D.N.; Gitau, M.W.; Pai, N.; Daggupati, P.; Gitau, M.W.; Member, A.; Moriasi, D.N. Hydrologic and Water Quality Models: Performance Measures and Evaluation Criteria. *Trans. ASABE* **2015**, *58*, 1763–1785. [[CrossRef](#)]
56. Brighenti, T.M.; Bonumá, N.B.; Grison, F.; de Almeida Mota, A.; Kobiyama, M.; Chaffe, P.L.B. Two Calibration Methods for Modeling Streamflow and Suspended Sediment with the SWAT Model. *Ecol. Eng.* **2019**, *127*, 103–113. [[CrossRef](#)]
57. Chow, V.T.; Maidment, D.R.; Mays, L.W. *Applied Hydrology McGraw-Hill International Editions*; McGraw-Hill Science/Engineering/Math: New York, NY, USA, 1988.
58. Subcommittee, H. *USGS Interagency Advisory Committee on Water Data*; Office of Water Data Coordination, US Geologic Survey: Reston, VA, USA, 1986. Available online: https://water.usgs.gov/osw/bulletin17b/dl_flow.pdf (accessed on 9 November 2022).
59. Mayo, T.L.; Lin, N. Climate Change Impacts to the Coastal Flood Hazard in the Northeastern United States. *Weather Clim. Extrem.* **2022**, *36*, 100453. [[CrossRef](#)]

Disclaimer/Publisher’s Note: The statements, opinions and data contained in all publications are solely those of the individual author(s) and contributor(s) and not of MDPI and/or the editor(s). MDPI and/or the editor(s) disclaim responsibility for any injury to people or property resulting from any ideas, methods, instructions or products referred to in the content.